Korean J. Chem. Eng., 37(8), 1387-1393 (2020)
DOI: 10.1007/s11814-020-0604-4

pISSN: 0256-1115
eISSN: 1975-7220

Composition-dependent catalytic activity of bimetallic PtPd dendrimer-encapsulated nanoparticles having an average size of 1.7 nm for hydrolytic dehydrogenation of ammonia borane

Youngwon Ju and Joohoon Kim†

Department of Chemistry, Research Institute for Basic Sciences, KHU-KIST Department of Converging Science and Technology, Kyung Hee University, Seoul 02447, Korea
(*Received 26 March 2020 • Revised 27 May 2020 • Accepted 4 June 2020*)

Abstract−We investigated composition-dependent catalytic activity of bimetallic PtPd dendrimer-encapsulated nanoparticles (DENs) that had a uniform size of ~1.7 nm for hydrolytic dehydrogenation of ammonia borane (AB). The PtPd DENs, composed of seven different Pt : Pd ratios, were synthesized using hydroxyl-terminated sixth-generation polyamidoamine dendrimers as a molecular template. The dendrimer-templating method allowed for synthesizing bimetallic PtPd DENs with controllable nanoparticle composition while fixing the size of the nanoparticles uniformly at ~1.7 nm. Compared with monometallic Pt and Pd DENs, the bimetallic PtPd DENs showed superior catalytic activity for the hydrolytic dehydrogenation of AB. Furthermore, the bimetallic PtPd DENs exhibited composition-dependent activity with the maximum activity (i.e., average turnover frequency=108.5±15.9 $mol_{H_2} \cdot mol_{atom\ Pt+Pd}^{-1} \cdot min^{-1}$) at a Pt : Pd ratio of 1 : 1 for the catalytic hydrolysis of AB.

Keywords: Dendrimer-encapsulated Nanoparticle (DEN), Hydrolytic Dehydrogenation, Ammonia Borane, Bimetallic PtPd Nanoparticles, Composition-dependent Catalysis

INTRODUCTION

Ammonia borane (AB, NH_3BH_3) has been one of the most promising hydrogen storage chemicals for on-board hydrogen storage applications owing to its high hydrogen capacity of 19.6 wt%, nontoxicity, and good stability [1,2]. AB can release hydrogen gas as a clean energy carrier via dehydrogenation pathways such as thermolysis, dehydrocoupling, and solvolysis (i.e., hydrolysis and alcoholysis) of AB [1,3]. In particular, the catalytic hydrolysis of AB has been considered attractive as an efficient means of rapid hydrogen release under mild conditions with high hydrogen selectivity for practical applications including fuel cells [4,5]. Therefore, various metallic nanoparticle catalysts have been suggested to identify and improve catalytic methods for hydrolyzing AB [4,6-9]. Bimetallic nanoparticles have attracted particular interest because bimetallization could make it possible to achieve new catalytic systems not obtainable with monometallic catalysts as well as to improve catalytic performance of monometallic counterparts [10-13]. For example, poly(*N*-vinyl-2-pyrrolidone)-stabilized PdPt nanoparticles have been reported for use in the catalytic hydrolysis of AB with an average turnover frequency (TOF) of 125 $mol_{H_2} \cdot mol_{cat}^{-1} \cdot min^{-1}$ [14]. Composition-specific activity of PdPt nanoparticles supported on electrospun polyacrylonitrile nanofibers has been also reported for the hydrolytic dehydrogenation of AB [15]. In addition, bimetallic PdPt nanocubes have been reported as a high-performance catalyst for the hydrolysis of AB [16]. Recently, more attention has been drawn to the synergistic catalysis of bimetallic PtPd nanoparticles in the hydrolysis of AB [17,18]. However, considering the complexity of most previous bimetallic nanoparticle catalysts in sizes, shapes, and support types, there is still a substantial need for efficient bimetallic catalysts with more uniform sizes and shapes in the absence of support synergy in order to better understand the effects of composition-specific bimetallization on the catalytic hydrolysis of AB.

Since zerovalent Cu nanoclusters were prepared using polyamidoamine (PAMAM) dendrimers as a molecular template [19,20], the use of dendrimer templates has been demonstrated to synthesize a variety of metallic nanoparticles encapsulated inside dendrimers (i.e., so-called dendrimer-encapsulated nanoparticles (DENs)) [21-25]. Unique features of dendrimers, highly branched and monodisperse polymers possessing a central core with repetitive branching units terminated with a large number of surface functional groups, makes DENs attractive catalysts for hydrogenation [26,27], dehydrogenation [28,29], 4-nitrophenol reduction [30], electrochemical oxygen reduction [31], and carbon-carbon coupling [32-34] (e.g., Heck, Suzuki, and Stille) reactions. In particular, well-defined structural features of dendrimers provide for high control over nanoparticle size, composition, and structure in dendrimer-templating synthesis, which is appropriate for the study of effects of the nanoparticle features on catalysis [35,36]. For example, size-specific catalytic activity of Pt DENs has been reported for enhanced oxygen reduction reaction [37]. In addition, composition-dependent activity of PtPd DENs has been reported for oxygen reduction reaction and hydrogenation of 13-cyclooctadine [38-40]. Interestingly, dendrimers have been also proposed as an attractive host of catalytic bimetallic nanoparticles such as PtNi and AgCo nanoparticles to study catalytic activity of the bimetallic nanoparticles in the hydro-

†To whom correspondence should be addressed.
E-mail: jkim94@khu.ac.kr

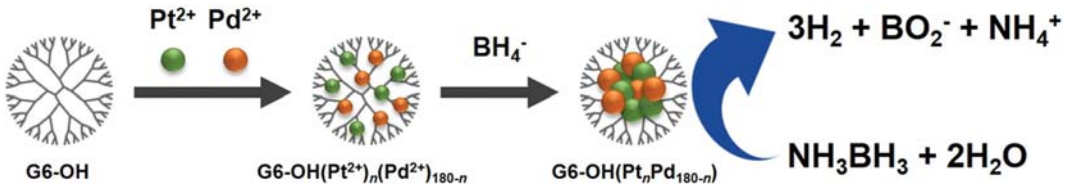

Scheme 1. Schematic illustration showing the syntheis of bimetallic PtPd DENs with different elemental composition and their use as catalysts for hydrolysis of AB.

lytic dehydrogenation of AB [29,41].

In this study, we investigated composition-dependent catalytic activity of bimetallic PtPd DENs of fairly uniform size (i.e., ~1.7 nm in diameter) for hydrolytic dehydrogenation of AB (Scheme 1). We synthesized seven different DENs by co-complexing different ratios of Pt^{2+} and Pd^{2+} precursor ions into the interiors of PAMAM dendrimers while fixing the total metal ions-to-dendrimer ratio at 180 : 1 and subsequent chemical reduction of the complexed metal ions. The resulting PtPd DENs were stable and soluble in water, and they exhibited different compositions subject to the molar ratio of the Pt^{2+} and Pd^{2+} precursors while having a uniform size of ~1.7 nm. The bimetallic PtPd DENs exhibited higher catalytic activity for the hydrolytic dehydrogenation of AB than did their monometallic counterparts (i.e., Pt and Pd DENs). Importantly, the catalytic activity of the PtPd DENs was controllable with different ratios of Pt and Pd in the bimetallic DENs; that is, the composition-dependent activity of the PtPd DENs can be optimized simply by adjusting the ratios of Pt and Pd precursor salts in dendrimer-templating synthesis. The highest activity for the catalytic hydrolysis of AB occurred at a Pt : Pd ratio of 1 : 1 over the different compositions of PtPd DENs having a uniform size of ~1.7 nm with a TOF of 108.5± 15.9 $mol_{H_2} \cdot mol_{atom\ Pt+Pd}^{-1} \cdot min^{-1}$ in the absence of catalyst supports.

EXPERIMENTAL

1. Chemicals and Materials

Hydroxyl-terminated sixth-generation polyamidoamine dendrimer (G6-OH), potassium tetrachloroplatinate(II) (K_2PtCl_4), potassium tetrachloropalladate(II) (K_2PdCl_4), sodium borohydride ($NaBH_4$), ammonia borane (AB, NH_3BH_3), and dialysis sack (MWCO of 12,000) were purchased from Sigma-Aldrich, Inc. (USA). Additionally, hydrogen chloride (HCl), nitric acid (HNO_3) were purchased from Daejung, Inc. (Korea). All aqueous solutions were prepared using deionized (DI) water (18 MΩ·cm) (aqua MAX Ultra 370, Younglin Instrument Co., Korea).

2. Synthesis and Characterization of DENs

Bimetallic PtPd DENs were synthesized in a similar way to the dendrimer-templating method reported previously [38,39,42]. Briefly, aqueous solutions of K_2PtCl_4 and K_2PdCl_4 were sequentially added to a 2 μM aqueous G6-OH solution. The molar ratio of the precursor Pt and Pd salts was adjusted to *n*:(180-*n*) where *n*=0, 30, 60, 90, 120, 150, and 180, while the final molar ratio of (total metal)-to-(G6-OH) was fixed at 180 : 1. The mixture was stirred for 72 h under ambient condition to ensure complete complexation of the precursor metal ions with the interior amines of G6-OH. This formed metal ion/G6-OH complexes that we denoted as G6-OH $(Pt^{2+})_n(Pd^{2+})_{180-n}$ (*n*=0, 30, 60, 90, 120, 150, and 180). Then, a ten-fold molar excess of $NaBH_4$ was added to the G6-OH$(Pt^{2+})_n(Pd^{2+})_{180-n}$ complex solution under vigorous stirring. This resulting solution was kept in a closed vial for 24 h under stirring to allow the complexed metal ions to be fully reduced. Finally, the resulting PtPd DEN solutions (i.e., G6-OH(Pt_nPd_{180-n}) (*n*=0, 30, 60, 90, 120, 150, and 180)) were dialyzed for 24 h using a cellulose dialysis sack (MWCO of 12,000) to remove impurities.

After the seven DENs (i.e., G6-OH(Pt_nPd_{180-n}) (*n*=0, 30, 60, 90, 120, 150, and 180)) were synthesized, they were subject to full characterization as follows. Transmission electron microscope (TEM) measurements were performed using a Tecnai G2 F30ST (FEI Co., USA) and a Titan Probe Cs (FEI Co., USA). TEM samples were prepared by dropping aqueous samples on 400 mesh carbon-coated copper grids (Ted Pella Inc., USA) and drying these in air. X-ray photoelectron spectroscopy (XPS) measurements were carried out with a K-Alpha X-ray photoelectron spectrometer (Thermo Scientific, USA) using Al Kα radiation (hν=1,486.6 eV). Inductively coupled plasma-atomic emission spectroscopy (ICP-AES) was performed to characterize the elemental composition of DENs using an iCAP™ 7200 spectrometer (Thermo Scientific, USA).

3. Catalytic Activity Measurement of DENs in Hydrolysis of AB

The catalytic activity of G6-OH(Pt_nPd_{180-n}) (*n*=0, 30, 60, 90, 120, 150, and 180) DENs was determined by measuring the rate of hydrogen generation in hydrolysis of AB at 298 K. The catalytic hydrolysis reaction was carried out in a laboratory-built dehydrogenation apparatus that was based on a 100 mL three-necked round bottom flask connected with a gas pressure transducer, thermal probes, a dropping funnel, and a gas purging tube. The middle and right necks of the flask were connected to a dropping funnel for introducing the AB reactant and a gas tube for purging with nitrogen, respectively. The left neck was connected to a gas pressure transducer (Extech SDL 700, Extech Instruments, USA) for real-time monitoring of pressure change due to generated hydrogen gas. The reaction temperature was controlled using a temperature controller (TC130P, MTops® Inc., Korea) and heating tapes (MTops® Inc., Korea) and monitored with thermal probes (MTops® Inc., Korea). Prior to the AB hydrolysis, an aqueous DENs solution was placed in the flask along with a magnetic stir bar. The flask was then thoroughly purged with nitrogen gas. After it was confirmed that the whole apparatus was tightly sealed and the reaction temperature was steady, 8 mL of aqueous AB solution (31.25 mM) was introduced into the flask using the dropping funnel under vigorous stirring (1,200 rpm) to initiate the AB hydrolysis; the amount of generated hydrogen gas was determined by measuring the increase in

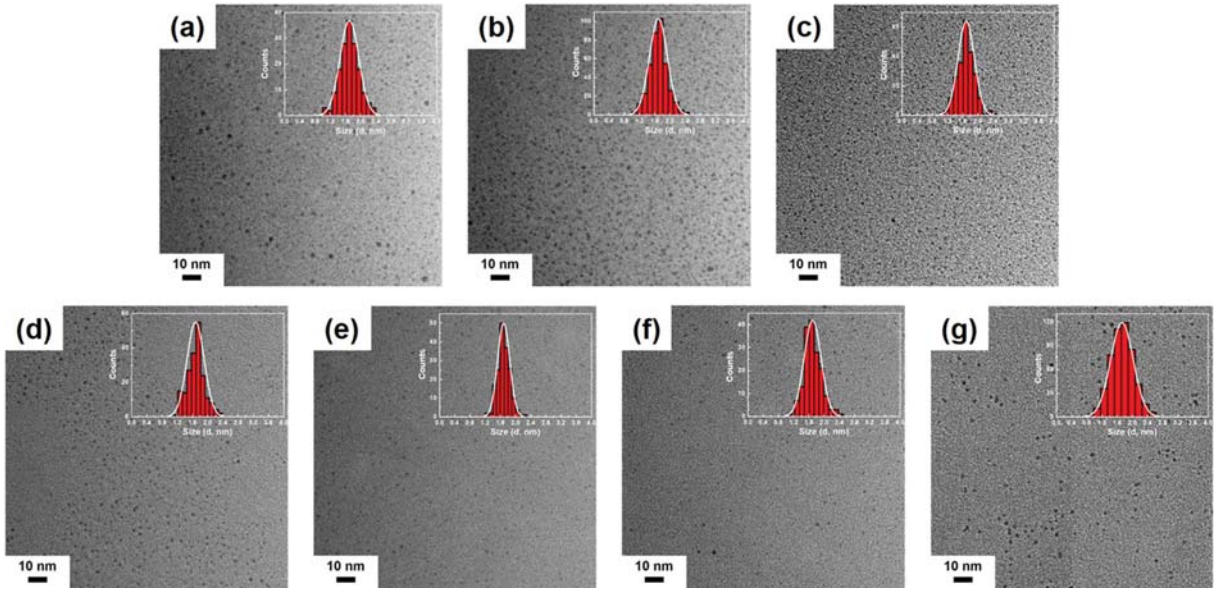

Fig. 1. TEM images of (a) G6-OH(Pd_{180}), (b) G6-OH($Pt_{30}Pd_{150}$), (c) G6-OH($Pt_{60}Pd_{120}$), (d) G6-OH($Pt_{90}Pd_{90}$), (e) G6-OH($Pt_{120}Pd_{60}$), (f) G6-OH ($Pt_{150}Pd_{30}$), and (g) G6-OH(Pt_{180}) DENs. Insets in panel show size-distribution histograms of the G6-OH(Pt_nPd_{180-n}) (n=0, 30, 60, 90, 120, 150, and 180).

the pressure inside the flask with the gas pressure transducer during the hydrolysis. The final concentration of catalytic DENs and AB was 400 nM and 25 mM, respectively.

RESULTS AND DISCUSSION

Seven different G6-OH(Pt_nPd_{180-n}) (n=0, 30, 60, 90, 120, 150, and 180) DENs were synthesized via co-complexation of Pt^{2+} and Pd^{2+} precursor ions (unless indicated otherwise, Pt^{2+} and Pd^{2+} ions are used to represent all possible complex ions) in the interior amines of G6-OH dendrimers and subsequent reduction of the ions complexed within the dendrimers [38,39,42]. In particular, the elemental composition of DENs was controlled by adjusting the molar ratio of precursor Pt and Pd salts to n:(180-n) where n=0, 30, 60, 90, 120, 150, and 180 during the DENs synthesis. Fig. 1 shows the TEM characterization of the resulting DENs (G6-OH(Pt_nPd_{180-n}) (n=0, 30, 60, 90, 120, 150, and 180)) in terms of average size and size distribution. The TEM images indicated that the seven different DENs, including both bimetallic PtPd DENs and monometallic counterparts (Pt and Pd DENs), were rarely aggregated and fairly monodisperse in size and shape, suggesting stabilization of the nanoparticles via their encapsulation inside the dendrimers as previously reported [42,43]. In particular, the average diameters of the DENs were quite uniform (~1.7 nm) and very close to the theoretical value of 1.73 or 1.72 nm calculated by assuming a spherical geometry of the nanoparticles containing 180 Pt or Pd atoms, respectively [38,44]. The uniform size of seven different DENs despite their different elemental compositions is attributable to the similar atomic diameters of Pt and Pd (i.e., 277 and 275 pm, respectively) [45]. Because of the fairly uniform size of the G6-OH(Pt_nPd_{180-n}) DENs, we expected that their catalytic activity in the hydrolytic dehydrogenation of AB, which is discussed later, would correlate directly with the compositions of the DENs.

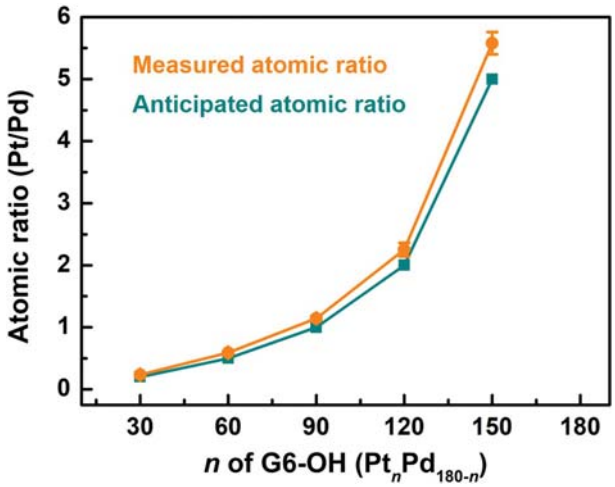

Fig. 2. Atomic ratios of Pt and Pd as a function of n values in G6-OH(Pt_nPd_{180-n}) (n=30, 60, 90, 120, and 150).

To elucidate the composition of bimetallic DENs, we conducted elemental quantification of both Pt and Pd with ICP-AES analysis of G6-OH(Pt_nPd_{180-n}) DENs. Fig. 2 shows the measured atomic ratio of Pt and Pd (i.e., Pt/Pd) in bimetallic DENs according to the molar ratios (i.e., n values in G6-OH(Pt_nPd_{180-n})) of the precursor Pt and Pd salts (in the present study, K_2PtCl_4 and K_2PdCl_4) used to synthesize the bimetallic DENs. The ICP-AES measurements verified that the measured atomic ratios of Pt and Pd agreed well with the anticipated values on the basis of the molar ratios of the precursor metal salts used for the synthesis, which is consistent with other bimetallic nanoparticles synthesized previously using dendrimer templating [41,42,46]. The elemental composition of bimetallic DENs was further confirmed with XPS measurements. Similar to the ICP-AES results, the XPS study of bimetallic DENs indicated that

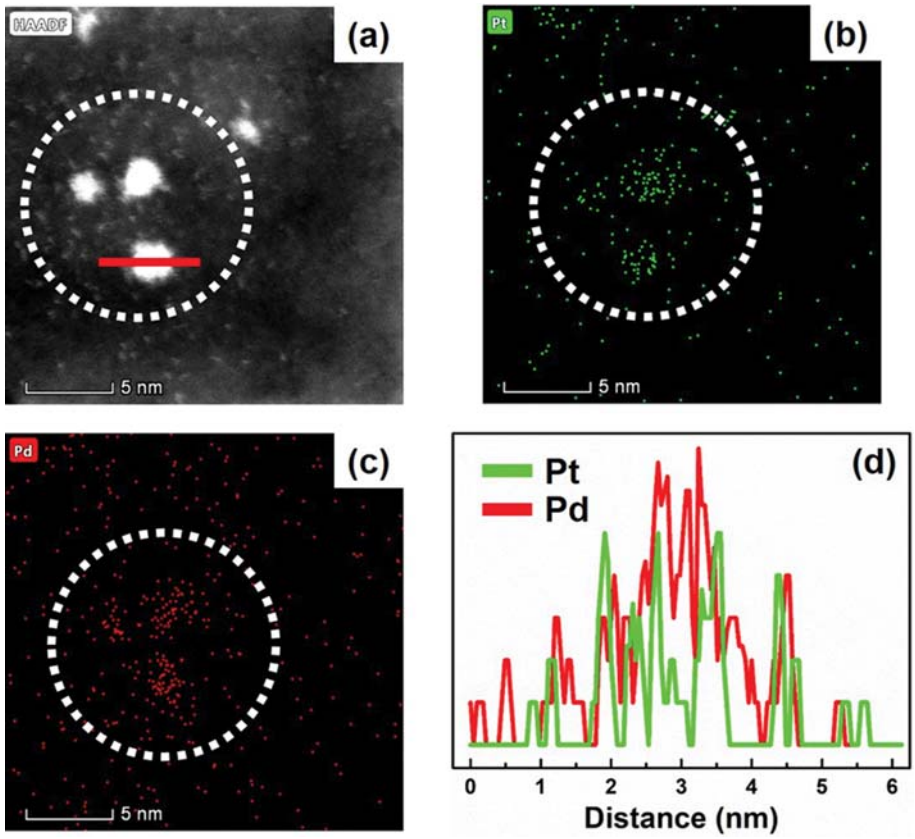

Fig. 3. (a) HAADF-STEM image and (b), (c) corresponding STEM-EDS elemental mapping images of Pt and Pd, respectively, for G6-OH ($Pt_{90}Pd_{90}$). (d) EDS line profile obtained along the solid red line shown in part (a).

the molar ratios of the precursor metal salts used for the synthesis were reflected in the actual compositions of the bimetallic DENs (Supplementary Material, Fig. S1 and Table S1). The XPS analysis of monometallic counterparts (i.e., Pt and Pd DENs) also verified the monometallic compositions of the DENs with only Pt or Pd (Supplementary Material, Fig. S1 and Table S1).

In addition, we performed elemental analysis of bimetallic DENs at the single-particle level to reveal the composition of bimetallic DENs. Fig. 3 shows a high-angle annular dark field-scanning transmission electron microscopy (HAADF-STEM) image and corresponding STEM-energy dispersive X-ray spectroscopy (STEM-EDS) elemental mapping images of a representative bimetallic DEN (e.g., G6-OH($Pt_{90}Pd_{90}$)). As shown in Fig. 3(d), the single-particle elemental mapping measurement of G6-OH($Pt_{90}Pd_{90}$) confirmed that both Pt and Pd were evenly present within the single nanoparticle, indicating that the G6-OH($Pt_{90}Pd_{90}$) DENs were bimetallic nanoparticles rather than physical mixtures of monometallic nanoparticles. It is also worth noting that the bimetallic nanoparticles eventually decomposed when they were exposed to electron beam irradiation during the STEM-EDS measurements, which restricted high-resolution elemental mapping of the nanoparticles as reported previously (Supplementary Material, Fig. S2) [47,48]. The crystalline structure of G6-OH($Pt_{90}Pd_{90}$) was also characterized by high-resolution transmission electron microscopy (HRTEM). A typical HRTEM image on the single G6-OH($Pt_{90}Pd_{90}$) DENs showed lattice fringes (Supplementary Material, Fig. S3), indicating the bimetallic nanoparticles were crystalline. The fringes with a lattice spacing of ~0.224 nm can be indexed to the {111} planes of a face-centered cubic (fcc) lattice when considering the values of lattice fringes for Pt (~0.226 nm) and Pd (~0.220 nm) [49,50]. The formation of a single-crystal PtPd bimetallic nanoparticle was attributable to the negligible lattice mismatch between Pt and Pd [51].

After confirming the controllable composition of G6-OH(Pt_nPd_{180-n}) (n=0, 30, 60, 90, 120, 150, and 180) DENs with a uniform size at ~1.7 nm, we quantitatively investigated the catalytic activity of G6-OH(Pt_nPd_{180-n}) DENs as a function of their elemental composition. Fig. 4(a) shows time-dependent profiles of hydrogen generation from aqueous AB at 298 K in the presence of G6-OH(Pt_nPd_{180-n}) DENs at a DENs/AB molar ratio of 1.6×10^{-5} by catalytic hydrolysis of AB. Both bimetallic PtPd DENs and monometallic counterparts catalyzed the hydrolytic AB dehydrogenation with the release of 3 molar equivalents of hydrogen per mole of AB, indicating complete generation of hydrogen from AB. The monometallic Pt DENs exhibited higher catalytic activity than that of the monometallic Pd DENs, indicating that Pt is more catalytic than Pd for the dehydrogenation of AB as reported previously [16,52]. But Pt DENs still required more than 26 min to complete the hydrolytic dehydrogenation of AB, whereas the time was significantly shortened in the presence of the bimetallic PtPd DENs. Moreover, the bimetallic PtPd DENs displayed different hydrolytic dehydrogenation rates depending on the elemental composition of PtPd DENs. The G6-OH($Pt_{90}Pd_{90}$) DENs in particular dramatically shortened the hydrolysis reaction

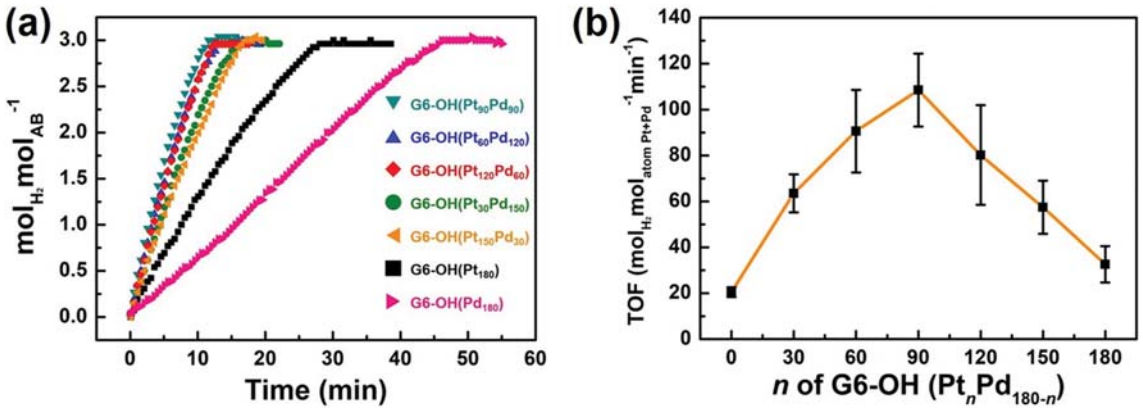

Fig. 4. (a) Time-dependent profiles of hydrogen generation from aqueous AB solutions in the presence of G6-OH(Pt_nPd_{180-n}) (n=0, 30, 60, 90, 120, 150, and 180) DENs. (b) TOF of G6-OH(Pt_nPd_{180-n}) (n=0, 30, 60, 90, 120, 150, and 180) DENs as a function of n in G6-OH(Pt_nPd_{180-n}). DENs/AB=1.6×10^{-5}.

time to less than 11 min, revealing the enhanced catalytic activity of G6-OH($Pt_{90}Pd_{90}$) with the hydrolytic dehydrogenation rate of 9.4 L_{H_2}·mol_{AB}^{-1}·min^{-1}. To quantify the catalytic activity of G6-OH (Pt_nPd_{180-n}) DENs, we measured the TOFs of hydrogen generation over G6-OH(Pt_nPd_{180-n}) DENs based on the initial rates of hydrogen generation at 298 K. Fig. 4(b) shows a volcano curve of TOFs as a function of n values in G6-OH(Pt_nPd_{180-n}) DENs, indicating a strong dependency of TOF on the composition of DENs. The G6-OH($Pt_{90}Pd_{90}$) DENs exhibited the highest catalytic activity with a TOF of 108.5±15.9 mol_{H_2}·$mol_{atom\ Pt+Pd}^{-1}$·min^{-1} for generating hydrogen from the catalytic hydrolysis of AB. The TOF of G6-OH($Pt_{90}Pd_{90}$) was much higher than those of monometallic Pt and Pd DENs (i.e., 32.5±7.9 and 20.5±2.1 mol_{H_2}·$mol_{atom\ Pt+Pd}^{-1}$·min^{-1}, respectively). Interestingly, the TOF of G6-OH($Pt_{90}Pd_{90}$) was also higher than that (i.e., 79.0±7.2 mol_{H_2}·$mol_{atom\ Pt+Pd}^{-1}$·min^{-1}) of a physical mixture of monometallic G6-OH(Pt_{90}) and G6-OH(Pd_{90}) DENs (Fig. 5), indicating that the high catalytic activity of G6-OH($Pt_{90}Pd_{90}$) arose from the synergistic effect of the bimetallic PtPd DENs [15,38,42]. The higher TOF of G6-OH($Pt_{90}Pd_{90}$), in comparison with that of the physical mixture of G6-OH(Pt_{90}) and G6-OH(Pd_{90}) DENs, further verified that the G6-OH($Pt_{90}Pd_{90}$) DENs are bimetallic as discussed in the

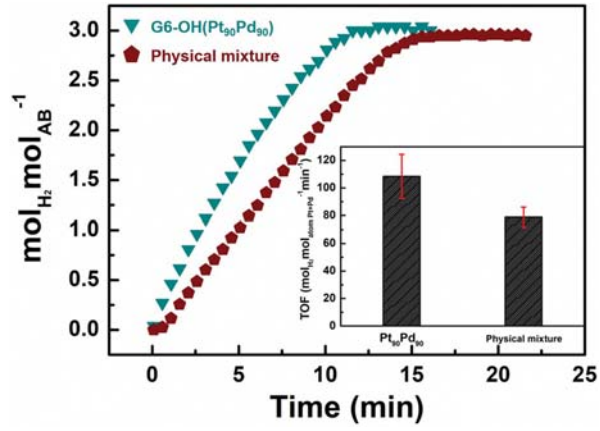

Fig. 5. Comparison of time-dependent profile of hydrogen generation from aqueous AB solutions in the presence of a physical mixture of monometallic G6-OH(Pt_{90}) and G6-OH(Pd_{90}) DENs with the time-dependent profile of bimetallic G6-OH ($Pt_{90}Pd_{90}$) shown in Fig. 4(a). Inset compares TOF of the bimetallic G6-OH($Pt_{90}Pd_{90}$) shown in Fig. 4(b) with that of the physical mixture of monometallic counterparts. DENs/AB=1.6×10^{-5}.

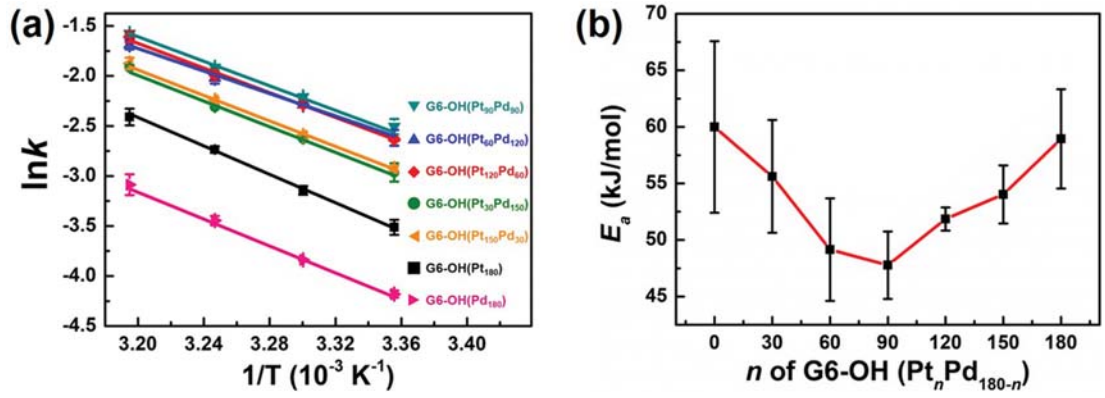

Fig. 6. (a) Arrhenius plots for G6-OH(Pt_nPd_{180-n}) (n=0, 30, 60, 90, 120, 150, and 180) DENs. (b) E_a of G6-OH(Pt_nPd_{180-n}) (n=0, 30, 60, 90, 120, 150, and 180) DENs as a function of n in G6-OH(Pt_nPd_{180-n}). DENs/AB=1.6×10^{-5}.

single-particle elemental mapping measurement of G6-OH($Pt_{90}Pd_{90}$) earlier [42].

To determine the activation energy (E_a) of G6-OH(Pt_nPd_{180-n}) (n=0, 30, 60, 90, 120, 150, and 180) DENs for the hydrolytic dehydrogenation of AB, we performed kinetic studies of AB hydrolysis in the presence of G6-OH(Pt_nPd_{180-n}) at different temperatures in the range of 298-313 K. After determining the values of rate constant k at different temperatures, we plotted the Arrhenius plots (i.e., ln$k$ vs. 1/T) for the G6-OH(Pt_nPd_{180-n}) DENs (Fig. 6(a)). From the Arrhenius plots, we calculated E_a for the AB hydrolysis catalyzed by the DENs (Fig. 6(b)), indicating different values of E_a depending on n in G6-OH(Pt_nPd_{180-n}) DENs. The different E_a values were in accordance with the strong dependency of TOF on the composition of the DENs as discussed earlier. In particular, the G6-OH($Pt_{90}Pd_{90}$) exhibited the lowest E_a of 47.8±3.0 kJ/mol for the AB hydrolysis of all the G6-OH(Pt_nPd_{180-n}) DENs we studied, suggesting the highest activity of G6-OH($Pt_{90}Pd_{90}$) for the catalytic hydrolysis of AB.

CONCLUSION

We have described composition-dependent catalytic activity of bimetallic PtPd DENs having a uniform size of ~1.7 nm for hydrolytic dehydrogenation of AB. We synthesized the DENs via co-complexation of Pt^{2+} and Pd^{2+} precursor ions at seven different molar ratios with the interior amines of G6-OH dendrimers and subsequent reduction of the precursor ions complexed within the dendrimers. The resulting DENs were composed of seven different Pt : Pd ratios, and their elemental compositions were adjustable simply by changing the molar ratios of the precursor Pt and Pd metal salts used for synthesizing the DENs while maintaining their sizes as uniform. Specifically, the DENs composed of different Pt : Pd ratios had a uniform size of ~1.7 nm, which allowed direct correlation of the DENs' compositions with the catalytic activity for the hydrolytic dehydrogenation of AB. The bimetallic PtPd DENs exhibited not only superior catalytic activity to that of the monometallic Pt and Pd DENs but also composition-dependent activity for the catalytic hydrolysis of AB. The highest catalytic activity of the bimetallic PtPd DENs occurred at a Pt : Pd ratio of 1 : 1 (i.e., G6-OH ($Pt_{90}Pd_{90}$)) with a TOF of 108.5±15.9 $mol_{H_2}\cdot mol_{atom\ Pt+Pd}^{-1}\cdot min^{-1}$ for the hydrolytic dehydrogenation of AB. This is a significant finding because the composition-dependent activity of PtPd DENs reflects the composition-specific bimetallization effect on the catalytic hydrolysis of AB without being compromised by heterogeneity of catalyst sizes.

ACKNOWLEDGEMENTS

This work was supported by the National Research Foundation of Korea funded by the Ministry of Science, ICT and Future Planning (NRF-2019M3E6A1065038 and NRF-2016M1A2A2936638) and the KIST Institutional Program (2Z05790-19-037).

SUPPORTING INFORMATION

Additional information as noted in the text. This information is available via the Internet at http://www.springer.com/chemistry/journal/11814.

REFERENCES

1. F. H. Stephens, V. Pons and R. T. Baker, *Dalton Trans.*, **25**, 2613 (2007).
2. N. C. Smythe and J. C. Gordon, *Eur. J. Inorg. Chem.*, **2010**, 509 (2010).
3. C. W. Hamilton, R. T. Baker, A. Staubitz and I. Manners, *Chem. Soc. Rev.*, **38**, 279 (2009).
4. H.-L. Jiang and Q. Xu, *Catal. Today*, **170**, 56 (2011).
5. Q. Xu and M. Chandra, *J. Alloys Compd.*, **446-447**, 729 (2007).
6. W.-W. Zhan, Q.-L. Zhu and Q. Xu, *ACS Catal.*, **6**, 6892 (2016).
7. D. Sun, V. Mazumder, Ö. Metin and S. Sun, *ACS Nano*, **5**, 6458 (2011).
8. Z.-H. Lu, J. Li, A. Zhu, Q. Yao, W. Huang, R. Zhou, R. Zhou and X. Chen, *Int. J. Hydrogen Energy*, **38**, 5330 (2013).
9. H. Dai, J. Su, K. Hu, W. Luo and G. Cheng, *Int. J. Hydrogen Energy*, **39**, 4947 (2014).
10. X. Peng, Q. Pan and G. L. Rempel, *Chem. Soc. Rev.*, **37**, 1619 (2008).
11. M. Sankar, N. Dimitratos, P. J. Miedziak, P. P. Wells, C. J. Kiely and G. J. Hutchings, *Chem. Soc. Rev.*, **41**, 8099 (2012).
12. F. Tao, *Chem. Soc. Rev.*, **41**, 7977 (2012).
13. A. Wang, X. Y. Liu, C.-Y. Mou and T. Zhang, *J. Catal.*, **308**, 258 (2013).
14. M. Rakap, *J. Power Sources*, **276**, 320 (2015).
15. Z. Zhang, Y. Jiang, M. Chi, Z. Yang, C. Wang and X. Lu, *RSC Adv.*, **5**, 94456 (2015).
16. A. J. Amali, K. Aranishi, T. Uchida and Q. Xu, *Part. Part. Syst. Charact.*, **30**, 888 (2013).
17. K. Yao, C. Zhao, N. Wang, T. Li and W. Lu, J. Wang, *Nanoscale*, **12**, 638 (2020).
18. Z. Wang, H. Zhang, L. Chen, S. Miao, S. Wu, X. Hao, W. Zhang and M. Jia, *J. Phys. Chem. C*, **122**, 12975 (2018).
19. M. Zhao, L. Sun and R. M. Crooks, *J. Am. Chem. Soc.*, **120**, 4877 (1998).
20. L. Balogh and D. A. Tomalia, *J. Am. Chem. Soc.*, **120**, 7355 (1998).
21. R. W. J. Scott, O. M. Wilson and R. M. Crooks, *J. Phys. Chem. B*, **109**, 692 (2005).
22. M. Zhao and R. M. Crooks, *Angew. Chem. Int. Ed.*, **38**, 364 (1999).
23. R. M. Crooks and M. Zhao, *Adv. Mater.*, **11**, 217 (1999).
24. R. M. Crooks, M. Zhao, L. Sun, V. Chechik and L. K. Yeung, *Acc. Chem. Res.*, **34**, 181 (2001).
25. V. S. Myers, M. G. Weir, E. V. Carino, D. F. Yancey, S. Pande and R. M. Crooks, *Chem. Sci.*, **2**, 1632 (2011).
26. Y. Niu, L. K. Yeung and R. M. Crooks, *J. Am. Chem. Soc.*, **123**, 6840 (2001).
27. M. Ooe, M. Murata, T. Mizugaki, K. Ebitani and K. Kaneda, *Nano Lett.*, **2**, 999 (2002).
28. C. Deraedt, R. Ye, W. T. Ralston, F. D. Toste and G. A. Somorjai, *J. Am. Chem. Soc.*, **139**, 18084 (2017).
29. D. Ke, Y. Li, J. Wang, L. Zhang, J. Wang, X. Zhao, S. Yang and S. Han, *Int. J. Hydrogen Energy*, **41**, 2564 (2016).
30. K. Esumi, R. Isono and T. Yoshimura, *Langmuir*, **20**, 237 (2004).
31. H. Ye and R. M. Crooks, *J. Am. Chem. Soc.*, **127**, 4930 (2005).

32. M. Ooe, M. Murata, T. Mizugaki, K. Ebitani and K. Kaneda, *J. Am. Chem. Soc.*, **126**, 1604 (2004).
33. Y. Li and M. A. El-Sayed, *J. Phys. Chem. B*, **105**, 8938 (2001).
34. J. C. Garcia-Martinez, R. Lezutekong and R. M. Crooks, *J. Am. Chem. Soc.*, **127**, 5097 (2005).
35. T. Cho, C. W. Yoon and J. Kim, *Langmuir*, **34**, 7436 (2018).
36. H. Lim, Y. Ju and J. Kim, *Anal. Chem.*, **88**, 4751 (2016).
37. K. Yamamoto, T. Imaoka, W.-J. Chun, O. Enoki, H. Katoh, M. Takenaga and A. Sonoi, *Nat. Chem.*, **1**, 397 (2009).
38. H. Ye and R. M. Crooks, *J. Am. Chem. Soc.*, **129**, 3627 (2007).
39. Y.-M. Chung and H.-K. Rhee, *Catal. Lett.*, **85**, 159 (2003).
40. Y.-M. Chung and H.-K. Rhee, *Catal. Surv. from Asia*, **8**, 211 (2004).
41. K. Aranishi, A. K. Singh and Q. Xu, *ChemCatChem*, **5**, 2248 (2013).
42. R. W. J. Scott, A. K. Datye and R. M. Crooks, *J. Am. Chem. Soc.*, **125**, 3708 (2003).
43. Y. Ju and J. Kim, *Chem. Commun.*, **51**, 13752 (2015).
44. H. Ye, J. A. Crooks and R. M. Crooks, *Langmuir*, **23**, 11901 (2007).
45. J.-C. Bertolini, *Appl. Catal. A-Gen.*, **191**, 15 (2000).
46. R. W. J. Scott, C. Sivadinarayana, O. M. Wilson, Z. Yan, D. W. Goodman and R. M. Crooks, *J. Am. Chem. Soc.*, **127**, 1380 (2005).
47. E. A. Lewis, T. J. A. Slater, E. Prestat, A. Macedo, P. O'Brien, P. H. C. Camargo and S. J. Haigh, *Nanoscale*, **6**, 13598 (2014).
48. C.-M. Wang, A. Genc, H. Cheng, L. Pullan, D. R. Baer and S. M. Bruemmer, *Sci. Rep.*, **4**, 3683 (2014).
49. W. P. Davey, *Phys. Rev.*, **25**, 753 (1925).
50. J. Wu, S. Shan, H. Cronk, F. Chang, H. Kareem, Y. Zhao, J. Luo, V. Petkov and C.-J. Zhong, *J. Phys. Chem. C*, **121**, 14128 (2017).
51. H. Zhang, M. Jin, H. Liu, J. Wang, M. J. Kim, D. Yang, Z. Xie, J. Liu and Y. Xia, *ACS Nano*, **5**, 8212 (2011).
52. M. Chandra and Q. Xu, *J. Power Sources*, **156**, 190 (2006).

Supporting Information

Composition-dependent catalytic activity of bimetallic PtPd dendrimer-encapsulated nanoparticles having an average size of 1.7 nm for hydrolytic dehydrogenation of ammonia borane

Youngwon Ju and Joohoon Kim[†]

Department of Chemistry, Research Institute for Basic Sciences, KHU-KIST Department of Converging Science and Technology, Kyung Hee University, Seoul 02447, Korea

(*Received 26 March 2020 • Revised 27 May 2020 • Accepted 4 June 2020*)

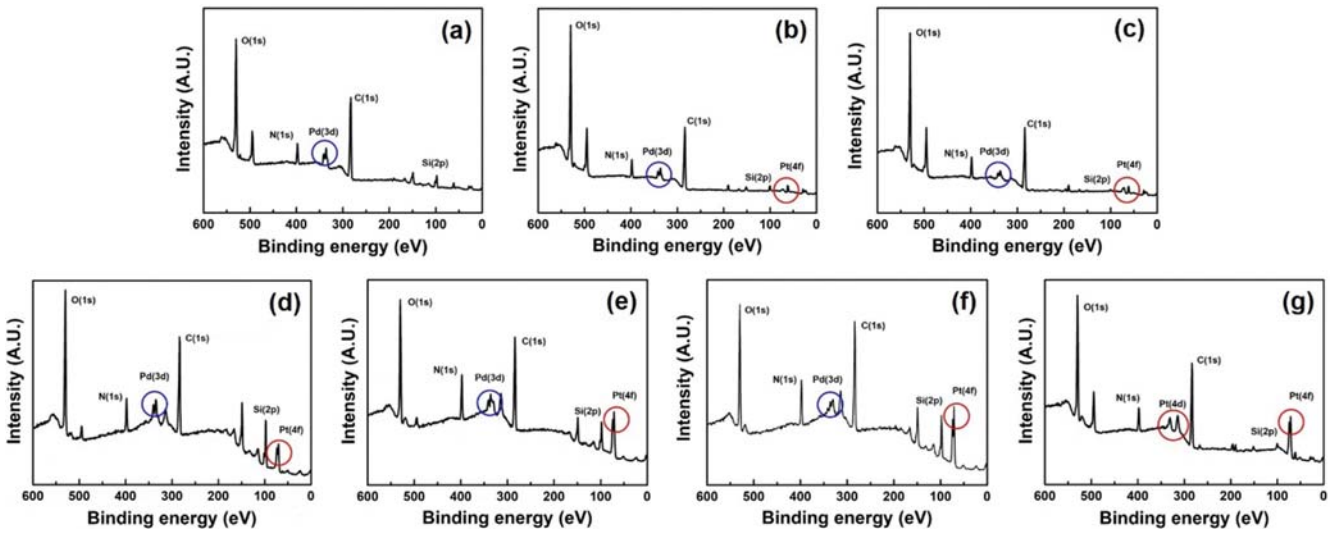

Fig. S1. Wide-scan XPS spectra of G6-OH(Pt_nPd_{180-n}) (*n*=0, 30, 60, 90, 120, 150, and 180) DENs. Blue and red circles indicate the characteristic XPS peaks of Pd and Pt, respectively.

Table S1. Atomic ratios obtained from XPS measurements for G6-OH(Pt_nPd_{180-n}) (*n*=0, 30, 60, 90, 120, 150, and 180) DENs

	G6-OH(Pd_{180})		G6-OH($Pt_{30}Pd_{150}$)		G6-OH($Pt_{60}Pd_{120}$)		G6-OH($Pt_{90}Pd_{90}$)		G6-OH($Pt_{120}Pd_{60}$)		G6-OH($Pt_{150}Pd_{30}$)		G6-OH(Pt_{180})	
	Pt (%)	Pd (%)	Pt (%)	Pd (%)	Pt (%)	Pd (%)	Pt (%)	Pd (%)	Pt (%)	Pd (%)	Pt (%)	Pd (%)	Pt (%)	Pd (%)
Measured atomic ratio	0	100	25.6±10.3	74.4±8.9	38.4±1.3	61.6±0.9	58.2±10.9	41.8±7.7	83.8±2.7	16.2±1.9	92.3±1.5	7.7±1.2	100	0
Anticipated atomic ratio	0	100	16.7	83.3	25	75	50	50	75	25	83.3	16.7	100	0

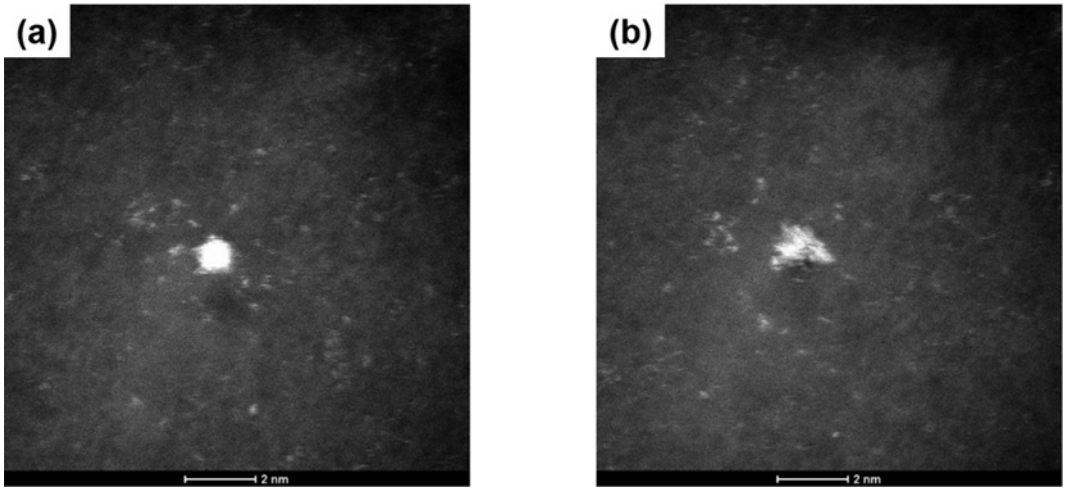

Fig. S2. High-angle annular dark field-scanning transmission electron microscopy (HAADF-STEM) images of bimetallic G6-OH($Pt_{90}Pd_{90}$) DENs before (a) and after (b) being exposed to electron beam irradiation during STEM measurements.

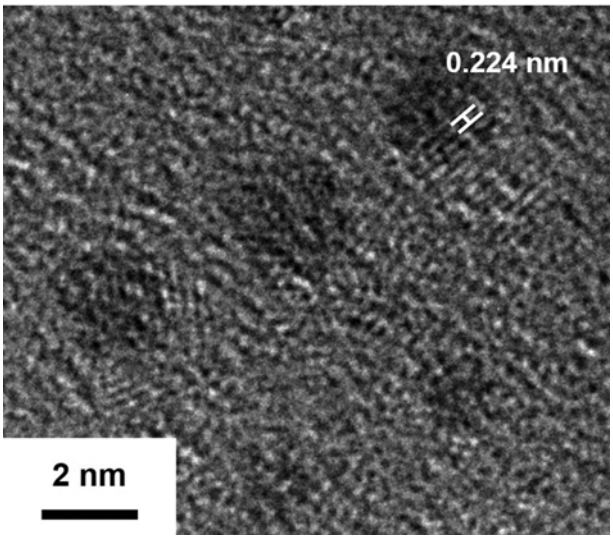

Fig. S3. High-resolution transmission electron microscopy (HRTEM) image of bimetallic G6-OH($Pt_{90}Pd_{90}$) DENs.